Nonlinear dynamics of vortex lattice formation in a rotating Bose-Einstein condensate

Kenichi Kasamatsu and Makoto Tsubota
Department of Physics, Osaka City University, Sumiyoshi-Ku, Osaka 558-8585, Japan

Masahito Ueda
Department of Physics, Tokyo Institute of Technology, Meguro-ku, Tokyo 152-8551, Japan
(Received 6 November 2002; published 26 March 2003)

We study the response of a trapped Bose-Einstein condensate to a sudden turn on of a rotating drive by numerically solving the two-dimensional Gross-Pitaevskii equation. A weakly anisotropic rotating potential excites a quadrupole shape oscillation and its time evolution is analyzed by a quasiparticle projection method. In a quadrupolar resonant regime, which depends on the trap anisotropy, simple periodic oscillations in surface-mode populations disappear and the system exhibits stochastic dynamics. In the presence of the phenomenological dissipation, an initially irrotational condensate is found to undergo damped elliptic deformation followed by unstable surface ripple excitations, some of which develop into quantized vortices that eventually form a lattice. Recent experimental results on the vortex nucleation should be explained not only by the dynamical instability but also by the Landau instability; the latter is necessary for the vortices to penetrate into the condensate.

DOI: 10.1103/PhysRevA.67.033610 PACS number(s): 03.75.Lm, 03.75.Kk, 05.30.Jp, 67.40.Db

I. INTRODUCTION

Since realization of Bose-Einstein condensates (BECs) of alkali-metal atomic gases, much attention has been focused on the dynamical phenomena associated with superfluidity. A remarkable feature reflecting superfluidity appears in the response to external rotation. Recent observation of a quantized vortex lattice in trapped BECs [1–4] confirmed the evidence of superfluidity. Madison *et al*. observed directly the nonlinear dynamical phenomena such as the vortex nucleation and lattice formation in a rotating condensate [5]. Such visualized results have greatly contributed to elucidation of static and dynamic properties of quantized vortices.

The dynamics of dilute BECs have been successfully described by the Gross-Pitaevskii (GP) mean-field model. For the quantized vortices in a trapped BEC, various theoretical studies have been made based on this model [6]. The mechanism of vortex nucleation in rotating trapped BECs is one of the important topics. Vortex nucleation of this system differs from that of a superfluid helium system in the ratio of the coherence length ξ to the system size L. In the former where $\xi \lesssim L$, vortex nucleation is related to the instability of collective excitations whose energy scale is set by the confining potential. In the latter where $\xi \ll L$, it is related to the local dynamics. A number of theoretical papers have discussed possible mechanisms of vortex nucleation [7–21]. However, only a few papers made full numerical analysis of the time-dependent GP equation, which is necessary to understand the results in Ref. [5]. Although the imaginary time propagation of the GP equation is a powerful scheme to find equilibrium states [9,13], the dynamical process toward such states cannot be revealed by this method. Feder *et al*. solved numerically the time-dependent GP equation in a rotating frame, but the motion of generated vortices remains turbulent, forming no vortex lattice [10]. Tsubota *et al.* [14] included a phenomenological dissipation into the GP equation to simulate a vortex lattice formation, obtaining the results consistent with those of Madison *et al.* [5]. Here a mechanism of the vortex lattice formation has been clarified as follows: (i) the condensate undergoes elliptic deformation, (ii) surface waves are excited at the boundary of the condensate, and (iii) quantized vortices enter the condensate from the boundary, forming a lattice.

What has remained to be clarified is the relation between the dynamical processes (i)–(iii) and intrinsic instabilities of a rotating condensate. There are two important instabilities for vortex nucleation, namely, the dynamical instability [12] and the Landau instability [7,9,15,16,18,19]. The former originates from the imaginary frequency of the excitation mode, giving rise to the exponential growth of the unstable mode even in the energy-conserving dynamics. The latter occurs when the excitation spectrum has negative eigenvalues in the rotating frame *and* when the system is subject to energy dissipation. These two instabilities often occur in different parameter regimes. Thus, one may ask which instability is important for actual experiments on vortex nucleation. While the vortex nucleation frequency found in the ENS experiments [1,5] appears to be consistent with that of the dynamical instability [12] and not with that of the Landau instability, our later analysis reveals that both instabilities play crucial roles in these experiments.

In this paper, we investigate theoretically the detailed dynamics of a BEC subject to external rotation by the numerical analysis of the two-dimensional GP equation, and address the above questions. The first issue of this paper concerns a response of a BEC to a sudden turn on of a rotating drive within the energy-conserving dynamics. The rotating potential excites chiefly the quadrupole surface mode with angular momentum $l=2$ and distorts the condensate into an ellipse. Because of the anisotropy of the trapping potential and the nonlinear atomic interaction, the different surface modes are coupled to each other, causing complicated nonlinear dynamics. To clarify the mode coupling, we use a quasiparticle projection method [22], which allows us to decompose the

macroscopic wave function into the condensate and noncondensate parts and determine the populations of each mode. We find that the condensate makes the simple periodic oscillation for most values of the rotation frequencies; populations of the excited modes restore their initial values in the sense of the Fermi-Pasta-Ulam recurrence [23]. In resonance of the quadrupole mode, however, the simple recurrence is replaced by chaotic behavior because of the dynamical instability of the rotating condensate [12]. An increase of the trap anisotropy expands the range of the rotation frequency for the resonance excitation. The chaotic dynamics yields violent density and phase fluctuations at the condensate surface. The generated surface ripples slightly increase of the total angular momentum, but they never develop into quantized vortices in the energy-conserving simulation.

Next, we consider the dissipative dynamics of the rotating BECs by extending our previous work [14]. This paper describes more detailed dynamics of the vortex lattice formation by following the time development of the condensate density and phase simultaneously. The GP equation with phenomenological dissipation explains the experimental results very well. The quasiparticle projection method is also applicable in the analysis of the dissipative dynamics; thus we can study what modes are excited during the dynamical process of vortex lattice formation. In the presence of dissipation, the excitations of surface ripple are caused by the surface modes with negative frequencies in the rotating frame [8]; the onset of this instability is given by the Landau criterion applied to the rotating BEC [7,9,15,16]. Numerical simulation shows that the surface ripples induced by the Landau instability certainly develop to quantized vortices. Therefore, it is concluded that vortex nucleation is essentially caused by the Landau instability. The ENS experiments [1] should be explained by the two-stage process: vortex nucleation by the Landau instability after the shape deformation by the dynamical instability.

This paper is organized as follows. Section II formulates our model that describes the dynamics of a rotating BEC in a harmonic trap. Section III studies the energy-conserving dynamics of a rotating BEC. The dynamics of the mode coupling is analyzed by the quasiparticle projection method. Section IV studies the dissipative dynamics of the vortex generation and lattice formation in detail, and makes some comments on the origin of the dissipation. Our results are compared with the experimental ones. Section V is devoted to the conclusion.

II. THE MODEL

A. Formulation of the problem

A BEC trapped in an external potential is described by a ''macroscopic wave function'' $\Psi(\mathbf{r},t)$ obeying the GP equation. In the frame rotating with the frequency Ω around the z axis the GP equation reads

$$i\hbar\frac{\partial\Psi}{\partial t}=\left(-\frac{\hbar^2}{2m}\nabla^2+V_{\mathrm{trap}}+V_{\mathrm{rot}}-\mu+g|\Psi|^2-\Omega L_z\right)\Psi. \tag{1}$$

Here $g=4\pi\hbar^2a/m$ represents the strength of interactions characterized by the s-wave scattering length $a>0$, μ the chemical potential, and $L_z=-i\hbar(x\partial_y-y\partial_x)$ the angular momentum. The wave function is normalized by the total particle number N as $\int d\mathbf{r}|\Psi|^2=N$. An external harmonic trapping potential has the form

$$V_{\mathrm{trap}}(\mathbf{r})=\tfrac{1}{2}m\{\omega_\perp^2(x^2+y^2)+\omega_z^2z^2\}, \tag{2}$$

and the potential that drives the rotation has the form

$$V_{\mathrm{rot}}(\mathbf{r})=\tfrac{1}{2}m\omega_\perp^2(\epsilon_x x^2+\epsilon_y y^2) \tag{3}$$

with the anisotropy parameters $\epsilon_x\neq\epsilon_y$; this form describes approximately the rotating potential used in the ENS experiments [1,5]. Such a rotating potential breaks the rotational symmetry, thus transferring the angular momentum into the condensate through the excitation of surface modes or the generation of vortices.

In order to reduce the system into the two-dimensional x-y space, we separate the degrees of freedom of the wave function as $\Psi(\mathbf{r},t)=\psi(x,y,t)\phi(z)$, obtaining the two-dimensional GP equation

$$\begin{aligned}i\hbar\frac{\partial\psi(x,y,t)}{\partial t}=\Bigg[&-\frac{\hbar^2}{2m}\left(\frac{\partial^2}{\partial x^2}+\frac{\partial^2}{\partial y^2}\right)+\frac{1}{2}m\omega_\perp^2\{(1+\epsilon_x)x^2\\&+(1+\epsilon_y)y^2\}-\mu+g\eta|\psi(x,y,t)|^2\\&-\Omega L_z\Bigg]\psi(x,y,t),\end{aligned} \tag{4}$$

where

$$\eta\equiv\frac{\int dz|\phi(z)|^4}{\int dz|\phi(z)|^2}, \tag{5}$$

and μ includes a constant arising from the integral of $\phi(z)$. The normalization of the two-dimensional wave function $\psi(x,y)$ is determined by the particle number $N_{2\mathrm{D}}$ per unit length along the z axis as

$$\int\int dxdy|\psi(x,y)|^2=N\left(\int dz|\phi(z)|^2\right)^{-1}=N_{2\mathrm{D}}. \tag{6}$$

It is convenient to introduce the scales characterizing the trapping potential; the length, time, and wave function are scaled as

$$x=a_h\tilde{x},t=\frac{\tilde{t}}{\omega_\perp},\psi=\sqrt{N_{2\mathrm{D}}}\frac{\tilde{\psi}}{a_h},$$

respectively, with $a_h=\sqrt{\hbar/2m\omega_\perp}$. Then the GP equation is reduced to a dimensionless form as

$$i\frac{\partial\psi}{\partial t}=\left[-\left(\frac{\partial^2}{\partial x^2}+\frac{\partial^2}{\partial y^2}\right)+\frac{1}{4}\{(1+\epsilon_x)x^2+(1+\epsilon_y)y^2\}-\mu+C|\psi|^2-\Omega L_z\right]\psi, \tag{7}$$

where $C=8\pi a\eta N_{2D}$ and the tilde is omitted for simplicity.

The two-dimensional approximation may be valid for the condensate in a "pancake-shaped" potential ($\lambda=\omega_z/\omega_\perp \gg 1$) or the central part of the condensate in a "cigar-shaped" potential ($\lambda<1$). These two types of situations yield different forms of the mean-field interaction strength C. For $\lambda\gg 1$ and $\hbar\omega_z$ larger than the interaction energy, $\phi(z)$ is approximated by the one-particle ground-state wave function in a harmonic potential:

$$\phi(z)=\left(\frac{1}{\sqrt{2\pi}a_{hz}}\right)^{1/2}\exp\left(-\frac{z^2}{4a_{hz}^2}\right) \tag{8}$$

with $a_{hz}=\sqrt{\hbar/2m\omega_z}=a_h/\sqrt{\lambda}$. Then, $N_{2D}=N$ and the parameter C becomes

$$C=8\pi aN\eta=4\sqrt{\pi\lambda}N\frac{a}{a_h}. \tag{9}$$

On the other hand, for a cigar-shaped condensate with $\lambda<1$ one can approximate the system with cylindrical configuration, i.e., translation symmetry along the z direction. By neglecting the spatial derivative term of the z component in Eq. (1), and the third term on the right-hand side of Eq. (2), the two-dimensional GP equation of Eq. (4) is obtained. Then the parameter C is written by

$$C=8\pi a\eta N_{2D}=8\pi aN\frac{\int|\phi(z)|^4dz}{\left(\int|\phi(z)|^2dz\right)^2}\simeq\frac{8\pi aN}{2R_z}. \tag{10}$$

Here R_z is assumed to be the Thomas-Fermi radius $\sqrt{2\mu/m\omega_z^2}$ along the z axis with the chemical potential evaluated at the parameter $\epsilon_{x,y}=0$ and $\Omega=0$:

$$\mu=\hbar\omega_\perp\left(\frac{15}{8}N\lambda\frac{a}{a_h}\right)^{2/5}. \tag{11}$$

The approximation for $\lambda<1$ is suitable for the ENS experiment [1] which was made under the cigar-shaped potential, where C [Eq. (10)] takes the value between 200 and 500. For the large condensate in the MIT experiment [2] $C\sim 10\,000$, though they did not use the cigar-shaped potential.

In the two-dimensional analysis, the effect of vortex bending [24,25] is not taken into account. Recent experiments [26] showed that the time scale of the vortex bending is found to be longer than 1 sec, which is much longer than the time scale of the dynamics of vortex lattice formation ($\sim$100 msec). We, therefore, consider our two-dimensional analysis effective for the present problem.

B. Numerical method

The numerical calculations of Eq. (7) are done using an alternating direction implicit method [27]. Defining a time step δ_t and space meshes $\delta_x=\delta_y=\delta$, and denoting the discrete wave function as $\psi_{j,k}^n=\psi(j\delta_x,k\delta_y,n\delta_t)$, $\psi_{j,k}^n$ develops into $\psi_{j,k}^{n+1}$ via the intermediate state $\psi_{j,k}^{n+(1/2s)}$ as

$$\psi_{j,k}^{n+1/2}=\psi_{j,k}^n-\frac{\Delta t}{\delta^2}(\partial_x^2\psi_{j,k}^{n+(1/2)}+\partial_y^2\psi_{j,k}^n)-i\Omega\Delta t(k\partial_x\psi_{j,k}^{n+(1/2)}-j\partial_y\psi_{j,k}^n)+\frac{\Delta t}{2}\{(V_{j,k}+C|\psi_{j,k}^{n+(1/2)}|^2)\psi_{j,k}^{n+(1/2)}+(V_{j,k}+C|\psi_{j,k}^n|^2)\psi_{j,k}^n\} \tag{12}$$

and

$$\psi_{j,k}^{n+1}=\psi_{j,k}^{n+(1/2)}-\frac{\Delta t}{\delta^2}(\partial_x^2\psi_{j,k}^{n+(1/2)}+\partial_y^2\psi_{j,k}^{n+1})-i\Omega\Delta t(k\partial_x\psi_{j,k}^{n+(1/2)}-j\partial_y\psi_{j,k}^{n+1})+\frac{\Delta t}{2}\{(V_{j,k}+C|\psi_{j,k}^{n+1}|^2)\psi_{j,k}^{n+1}+(V_{j,k}+C|\psi_{j,k}^{n+(1/2)}|^2)\psi_{j,k}^{n+(1/2)}\}. \tag{13}$$

Here we denote $\Delta t\equiv\delta_t/2i$, $\partial_x\psi_{j,k}^n\equiv(\psi_{j+1,k}^n-\psi_{j-1,k}^n)/2$, $\partial_x^2\psi_{j,k}^n\equiv\psi_{j+1,k}^n-2\psi_{j,k}^n+\psi_{j-1,k}^n$, and $V_{j,k}=\{(1+\epsilon_x)(j\delta)^2+(1+\epsilon_y)(k\delta)^2\}/4$. We used the $[-128\leqslant j,k\leqslant+128]$ discretized space for the two-dimensional numerical simulation. The time step $\delta_t=1.0\times10^{-3}$ is sufficient to ensure the numerical stability over sufficiently long propagation.

III. QUADRUPOLE OSCILLATION OF A ROTATING BEC

A. Time development of the deformation parameter

We start by discussing the time evolution from a stationary solution in a nonrotating trap. We turn on a rotating drive following the experimental procedure of Madison *et al.* [5]. The rotation with a frequency Ω starts at $t=0$, and the trap anisotoropy $\epsilon=\{(1+\epsilon_x)-(1+\epsilon_y)\}/\{(1+\epsilon_x)+(1+\epsilon_y)\}$ is increased rapidly from zero to its final value 0.025 in 20 msec, where ϵ_y is fixed to be zero. The strength of interaction C is set to be 500, corresponding to $a=5.77$ nm, $N=3\times10^5$, and $\omega_z=11.8\times2\pi$, $\lambda=\omega_\perp/\omega_z=9.2$ [5]. The unit of length is $a_h=\sqrt{\hbar/2m\omega_\perp}=0.728$ μms and the period of the trap 9.21 msec.

A rapid modulation of the trapping anisotropy induces an elliptic oscillation of the condensate. The elliptic oscillation is characterized by the deformation parameter [5,28]

$$\alpha=-\Omega\frac{\langle x^2\rangle-\langle y^2\rangle}{\langle x^2\rangle+\langle y^2\rangle}, \tag{14}$$

where $\langle A\rangle$ means $\int dxdy\,\psi^*A\psi$. The time evolution of α for several values of Ω is shown in Fig. 1. For relatively small

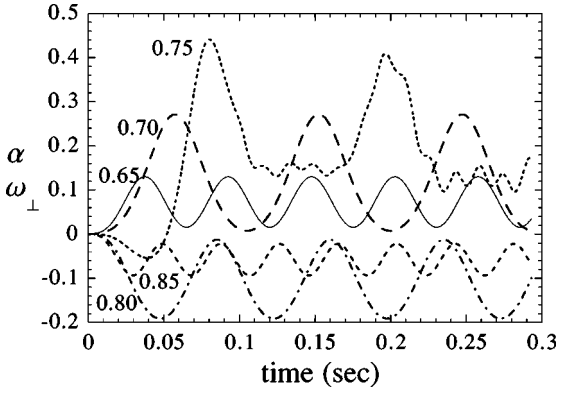

FIG. 1. Time evolution of the deformation parameter α for $\Omega/\omega_\perp = 0.65$, 0.70, 0.75, 0.80, and 0.85. Note that α shows aperiodic behavior at $\Omega/\omega_\perp = 0.75$, where the rotating drive resonantly hits the quadrupole mode.

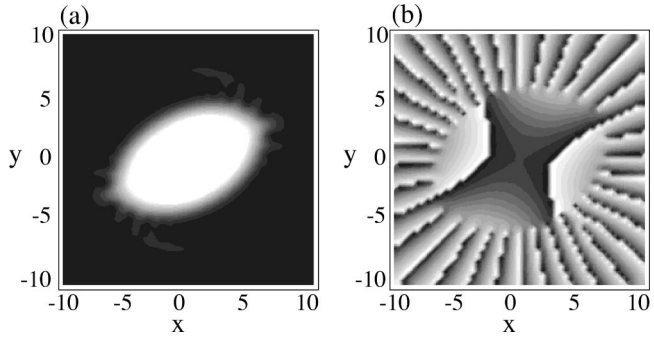

FIG. 2. The density profile (a) and phase profile (b) of the condensate with $\Omega/\omega_\perp = 0.75$ at 105 msec. In (b), the value of the phase changes continuously from 0 (black) to 2π (white). There appear some lines, where the phase changes discontinuously from black to white. These lines correspond to the branch cuts between the phases 0 and 2π, and their apexes around which the value of the phase rotates continuously from 0 to 2π represent phase defects, i.e., quantized vortices.

values of Ω, α undergoes a simple periodic oscillation with positive values; the initial axisymmetric condensate is elongated along the y axis because of the small trap anisotropy ϵ ($\epsilon_x > \epsilon_y$). As Ω increases from zero, both the amplitude and the period increase gradually, leading to the large amplitude oscillation near $\Omega = 0.7\omega_\perp$. For $\Omega = 0.75\omega_\perp$, however, α shows aperiodic behavior as shown in Fig. 1. As Ω increases further, the periodicity is restored, but the sign of α changes to negative and its absolute value become smaller and smaller. The negative α means that the longer axis of the condensate ellipse is perpendicular to the longer axis of the anisotropic trap.

This shape oscillation mainly consists of the collective surface mode with angular momentum $l = 2$, i.e., quadrupole mode. In the Thomas-Fermi limit, the dispersion relation for the surface mode reduces to $\omega_l = \sqrt{l}\omega_\perp$ [29]. Due to the centrifugal term $-\Omega L_z$, the surface-mode frequency is shifted by $-l\Omega$. For $l = 2$, hence, it is expected that the quadrupole mode is resonantly excited at $\Omega/\omega_\perp = \sqrt{2}/2 \simeq 0.707$. As discussed later, the single resonance does not occur because the quadrupole mode couples with various higher-energy modes through the nonlinear interaction, giving rise to the complicated dynamics. We find that for a range of the rotation frequency $0.72 < \Omega/\omega_\perp < 0.78$, the oscillation becomes irregular. The deviation from the pure resonance frequency $\Omega/\omega_\perp = 0.707$ is due to the effect of the trap anisotropy and the nonlinear interaction [see Eq. (23)].

Figure 2 shows the profile of the condensate density $|\psi(x,y,t)|^2$ and that of the phase $\theta(x,y,t) = \tan^{-1}(\mathrm{Im}\psi/\mathrm{Re}\psi)$ $(0 < \theta < 2\pi)$ when the irregular oscillation occurs. On the surface of the condensate, there appear surface ripples, which are violent short-wavelength density fluctuation. In addition, the phase profile shows that many phase singularities, i.e., quantized vortices, come into the condensate surface, while inside the condensate the phase features the form of the quadrupoler flow [9,28]. Since the phase singularities lie on the outskirts of the condensate where the amplitude $|\psi|$ is very small, they hardly contribute to both the energy and the angular momentum. Such phase singularities, named ''ghost vortices'' in our previous paper [14], are located in the density hollows produced by the surface ripples.

In the energy-conserving dynamics, such irregular dynamics are caused by the dynamical instability associated with the imaginary frequency of the excitation modes. Sinha and Castin [12] made a linear stability analysis of an oscillating condensate with a quadrupolar *ansatz*, and found the growth of the fluctuation to be described by polynomials of degree $n = 3$ around $\Omega/\omega_\perp = 0.73$. They proposed that the associated dynamical instability triggers vortex nucleation in a condensate rotating in an anisotropic harmonic potential. However, Fig. 2 suggests that the generated surface ripples should be described by polynomials with degrees higher than $n = 3$. Thus, we also make a linear stability analysis for $n = 4$ and 8 by following Ref. [12], and find that the growth rates of these higher-order modes are as high as $n = 3$. Hence, the dynamical instability excites such higher-order excitation modes, generating the surface ripples. These ripples slightly increase the total angular momentum because of the presence of ghost vortices, but they never penetrate into the condensate to form a lattice. Therefore, it is concluded that the dynamical instability alone does not lead to ''vortex nucleation'' as observed in the ENS experiments. In Sec. IV, we will show that the dissipation-assisted instability can make the surface ripples develop into the quantized vortices.

B. Quasiparticle projection method

The dynamics of the elliptic oscillation can be well explained by decomposing the whole dynamics into an assembly of fundamental excitation modes. The quasiparticle projection method, developed by Morgan *et al.* to study the nonlinear mixing of collective excitations [22], enables us to decompose a wave function into a condensate and noncondensate modes, and monitor the time evolution of their populations. Here we will use this method to study the time development of the surface modes excited by the anisotropic rotating trap.

To construct the mode functions for the projection, we use the solution of the time-independent GP equation with a nonrotating axisymmetric trap

$$\left[-\frac{d^2}{dr^2}-\frac{1}{r}\frac{d}{dr}+\frac{r^2}{4}+C|\psi_g|^2\right]\psi_g(r)=\mu\psi_g(r), \quad (15)$$

where ψ_g corresponds to the initial nonvortex state in our simulation. The quasiparticle mode functions $u_i(\mathbf{r})=u_i(r)e^{il\theta}$ and $v_i(\mathbf{r})=v_i(r)e^{il\theta}$ are obtained by the Bogoliubov-de Gennes equations

$$\left[-\left(\frac{d^2}{dr^2}+\frac{1}{r}\frac{d}{dr}-\frac{l^2}{r^2}\right)+\frac{r^2}{4}-\mu+2C|\psi_g|^2\right]u_i(r)+C\psi_g^2 v_i(r)=\omega_i u_i(r), \quad (16a)$$

$$\left[-\left(\frac{d^2}{dr^2}+\frac{1}{r}\frac{d}{dr}-\frac{l^2}{r^2}\right)+\frac{r^2}{4}-\mu+2C|\psi_g|^2\right]v_i(r)+C\psi_g^{*2}u_i(r)=-\omega_i v_i(r). \quad (16b)$$

The mode functions are subject to the orthogonality and symmetry relations

$$\int d^2r\{u_i(\mathbf{r})u_j^*(\mathbf{r})-v_i(\mathbf{r})v_j^*(\mathbf{r})\}=\delta_{ij}, \quad (17a)$$

$$\int d^2r\{u_i(\mathbf{r})v_j^*(\mathbf{r})-v_i(\mathbf{r})u_j^*(\mathbf{r})\}=0. \quad (17b)$$

Following the method of Ref. [22], we introduce a set of excitations that are orthogonal to ψ_g. This is achieved by projecting out the overlap with ψ_g from the solutions of the Bogoliubov-de Genne equations, the resulting quasiparticle wave functions being defined by

$$\tilde{u}_i(\mathbf{r})=u_i(\mathbf{r})-c_i\psi_g(\mathbf{r}), \quad (18a)$$

$$\tilde{v}_i^*(\mathbf{r})=v_i^*(\mathbf{r})+c_i^*\psi_g(\mathbf{r}), \quad (18b)$$

where $c_i=\int d^2\mathbf{r}[\psi_g^* u_i]=-\int d^2\mathbf{r}[\psi_g v_i]$. The orthogonal relations Eq. (17) still hold for these modified wave functions. The wave function can be expanded as

$$\psi(\mathbf{r},t)=\{1+b_g(t)\}\psi_g(\mathbf{r})+\sum_{i>0}\{\tilde{u}_i(\mathbf{r})b_i(t)+\tilde{v}_i^*(\mathbf{r})b_i^*(t)\}. \quad (19)$$

It is easy to show that $1+b_g$ and b_i satisfy the relations

$$1+b_g(t)=\int d^2r\psi_g^*(\mathbf{r})\psi(\mathbf{r},t), \quad (20)$$

$$b_i(t)=\int d^2r\{\tilde{u}_i^*(\mathbf{r})\psi(\mathbf{r},t)-\tilde{v}_i^*(\mathbf{r})\psi^*(\mathbf{r},t)\}. \quad (21)$$

The populations of the ground state and the excitation are given by $|1+b_g|^2$ and $|b_i|^2$.

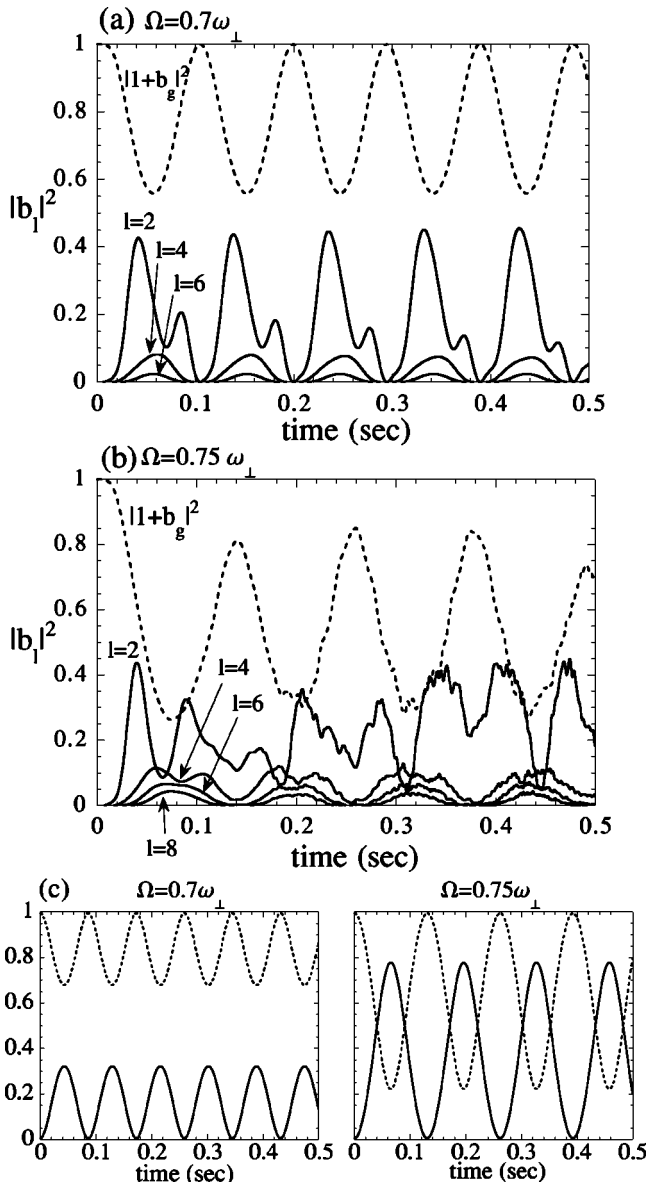

FIG. 3. Time evolution of the surface mode populations $|b_l|^2$ for (a) $\Omega/\omega_\perp=0.7$ and (b) $\Omega/\omega_\perp=0.75$. (c) represents the time evolution of $|1+b_g|^2$ (dashed curve) and $|b_2|^2$ (solid curve) in the two-mode approximation.

In the following discussion, we take only those mode functions that carry angular momentum l but do not possess any radial node, i.e., surface modes. Here the index i of $\tilde{u}_i$ and $\tilde{v}_i$ is replaced with l. For $l\neq 0$, the overlap integral c_l vanishes because $\int_0^{2\pi}d\theta e^{il\theta}=0$, so that $\tilde{u}_l=u_l$ and $\tilde{v}_l=v_l$. Since our system has even parity for the spatial coordinate, no surface modes with odd l are excited.

C. Fermi-Pasta-Ulam recurrence and chaotic dynamics

By using Eq. (21), we project the time evolution of the excitation modes $|b_l|^2$ with $l=2,4,\ldots,20$ from $\psi(\mathbf{r},t)$. Figure 3(a) shows the time evolution of $|b_2|^2$, $|b_4|^2$, $|b_6|^2$, and $|1+b_g|^2$ for $\Omega=0.7\omega_\perp$; other $|b_l|^2$'s are negligibly small.

The rotating potential of Eq. (3) dominantly excites the $l=2$ mode which causes the elliptic deformation. The small populations of higher modes ($l=4,6,\ldots$) also appear following the increase of $|b_2|^2$. After a certain period of time populations of all excited modes return to the initial values almost completely. This simple recurrence repeats periodically in time.

For $\Omega=0.75\omega_\perp$, the evolution is somewhat complicated as illustrated in Fig. 3(b). The recurrence is no longer complete, but some quasiperiodicity still remains. As compared with the simple recurrence dynamics, the depletion of the ground-state population becomes remarkably large, which means that more higher-energy modes are excited. The superposition of such higher-energy modes produces the surface ripples in the condensate density as shown in Fig. 2.

From a general point of view, we face the problem known as the Fermi, Pasta, and Ulam recurrence phenomenon [23]. They studied statistical behavior in the chain of nonlinearly coupled oscillators, and found a quasiperiodic behavior of this system characterized by returns of the energy to the initial excited mode. Later, it was shown that there exists a threshold for the onset of ''stochastization'' which is brought by high-energy excitations. For BECs in an anisotropic potential, the nonlinearities inside the condensate may give rise to the stochasticity in its time evolution [30–32].

D. Two-mode analysis

The simple analysis of the equation of motion for the quasiparticle population helps us understand the behavior of Figs. 3(a) and 3(b). Substituting Eq. (19) into Eq. (7), we get

$$i\frac{\partial b_g}{\partial t}=\int d^2r\,\psi_g^* V_{\rm rot}(\psi_g+\Delta)+C\int d^2r[(b_g+b_g^*)|\psi_g|^4 +2|\Delta\psi_g|^2+\Delta^2\psi_g^{*2}+\Delta|\Delta|^2\psi_g^*], \tag{22}$$

$$\begin{aligned} i\frac{\partial b_l}{\partial t}=&(\omega_l-l\Omega)b_l(t)+\int d^2r u_l^* V_{\rm rot}(\psi_g+\Delta)\\ &+C\int d^2r u_l^*[2|\Delta|^2\psi_g+\Delta^2\psi_g^*+\Delta|\Delta|^2\\ &+|\psi_g|^2\psi_g(b_g+b_g^*)]+\int d^2r v_l^* V_{\rm rot}(\psi_g+\Delta^*)\\ &+C\int d^2r v_l^*[2|\Delta|^2\psi_g^*+\Delta^{*2}\psi_g+\Delta^*|\Delta|^2\\ &+|\psi_g|^2\psi_g^*(b_g+b_g^*)], \end{aligned} \tag{23}$$

where $\Delta=b_g\psi_g+\Sigma_l\{u_l(\mathbf{r})b_l(t)+v_l^*(\mathbf{r})b_l^*(t)\}$ and $V_{\rm rot}=(\epsilon_x x^2+\epsilon_y y^2)/4$. The presence of $V_{\rm rot}$ makes the integrals $\int d^2r\,\psi_g^* V_{\rm rot}u_l$ or $\int d^2r u_{l'}^* V_{\rm rot}v_l\cdots$ finite, and these terms are reduced to the form $T_0\delta_{l,l'}+T_1\delta_{l,l'-2}+T_2\delta_{l,l'+2}$ after the integral of θ component (if $\epsilon_x=\epsilon_y$, the off-diagonal terms vanishes). Hence, the ground state is coupled directly only to the $l=2$ mode in Eq. (22) through $V_{\rm rot}$. The remaining terms with C couple the various modes with the same parity to each other, resulting in a complicated time evolution.

As seen in Fig. 3(a), the dominant contribution to the dynamics comes from the change of the populations $|1+b_g|^2$ and $|b_2|^2$. To understand the basic properties, we take only terms with $l=0$ and 2 (two-mode approximation). In addition, we neglect the contribution of $v_2(r)$, because this term represents the excitation traveling oppositely to the rotation. Then Eqs. (22) and (23) reduce to

$$i\frac{\partial b_g}{\partial t}=T_{00}(1+b_g)+P_{00}\{2{\rm Re}(b_g)+|b_g|^2\}(1+b_g) +P_{02}(1+b_g)|b_2|^2+T_{02}b_2, \tag{24a}$$

$$i\frac{\partial b_2}{\partial t}=(\omega_2-2\Omega+T_{22})b_2+P_{22}|b_2|^2b_2+P_{02}\{2{\rm Re}(b_g) +|b_g|^2\}b_2+T_{02}(1+b_g), \tag{24b}$$

where

$$T_{00}=\int d^2r\,\psi_g^* V_{\rm rot}\psi_g,$$

$$T_{22}=\int d^2r u_2^* V_{\rm rot}u_2 T_{02}=\int d^2r\,\psi_g^* V_{\rm rot}u_2 =\int d^2r u_2^* V_{\rm rot}\psi_g,$$

$$P_{00}=C\int d^2r|\psi_g|^4,$$

$$P_{22}=C\int d^2r|u_2|^4,$$

$$P_{02}=2C\int d^2r|\psi_g|^2|u_2|^2.$$

It is convenient to represent the complex values b_g and b_2 in terms of the amplitude and the phase as $1+b_g=|1+b_g|e^{i\theta_g}$ and $b_2=|b_2|e^{i\theta_2}$. Since the total population $|1+b_g|^2+|b_2|^2$ is a constant of motion, Eqs. (24) have two variables: population difference $p=|1+b_g|^2-|b_2|^2$ and relative phase $\theta=\theta_g-\theta_2$. Then, Eqs. (24) reduce to

$$\frac{dp}{dt}=2T_{02}\sqrt{1-p^2}\sin\theta, \tag{25}$$

$$\frac{d\theta}{dt}=Up-T_{02}\frac{2p}{\sqrt{1-p^2}}\cos\theta-\Delta\omega \tag{26}$$

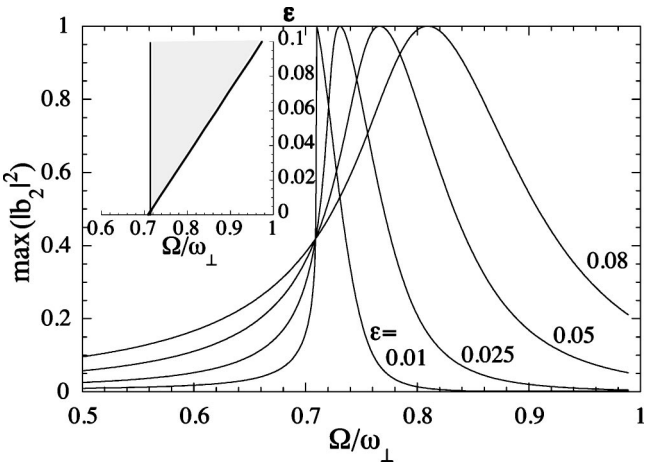

FIG. 4. The dependence of the maximum of $|b_2|^2$ on $\Omega/\omega_\perp$ in the two-mode approximation for $\epsilon=0.01$, 0.025, 0.05, and 0.08. The shaded region in the inset shows the parameter region in which the large amplitude oscillation with $\max(|b_2|^2)>0.4$ occurs.

with the conserved Hamiltonian

$$H(p,\theta)=\tfrac{1}{2}Up^2+2T_{02}\sqrt{1-p^2}\cos\theta-\Delta\omega p, \qquad (27)$$

where $U=(P_{00}+P_{22}-2P_{02})/2$ and $\Delta\omega=\omega_2-2\Omega+T_{22}-T_{00}+U$. These formula are the same with those used in the Josephson dynamics of the condensate in a double-well potential, and the exact solution of $p(t)$ is expressed by the Weierstrassian elliptic function [33]. For $C=500$, we numerically find as $\omega_2=1.438\omega_\perp$, $U=-0.05$, $\delta\omega=\omega_2-2\Omega+3\epsilon-0.05$ and $T_{02}=1.14\epsilon$ from the calculated ψ_g and u_2. The solutions of Eqs. (25) and (26) with these parameter values are shown in Figs. 3(c). The periodicity and the amplitude of $|1+b_g|^2$ reproduce well the results of the GP equation.

Figure 4 shows the dependence of the maximum of $|b_2|^2$ on $\Omega/\omega_\perp$. The maximum grows near $\Omega=0.7\omega_\perp$. Note that as ϵ increases the peak is shifted from the pure $l=2$ resonance frequency $\Omega=\omega_2/2=0.719\omega_\perp$ to the larger value of Ω. The dynamics of the GP equation does not show pronounced resonance of $|b_2|^2$ because the transition into higher energy modes occurs. For $\epsilon=0.025$, we found that the chaotic oscillation occurs in $0.72<\Omega<0.78$, which corresponds to the range where the maximum of $|b_2|^2$ exceeds 0.4 in Fig. 4. Following this criterion, we obtain the $\Omega-\epsilon$ parameter region where the large amplitude oscillation is expected, as shown in the inset of Fig. 4 (shaded region). In this region, the mode coupling via the nonlinear interaction becomes important, leading to chaotic dynamics. We confirm by the numerical simulation that the simple recurrence is indeed lost in this region. We will discuss the relevance of such a nonlinear coupling to vortex nucleation in Sec. IV E

IV. DYNAMICS OF VORTEX LATTICE FORMATION

In this section, we focus on the dissipative dynamics of a trapped condensate following the sudden turn on of rotation. The dissipation is necessary to simulate the dynamics of vortex lattice formation by the GP equation, because a vortex lattice corresponds to a local minimum of the total energy in the configuration space [34,35]. Preliminary results were reported in Ref. [14]. This section deals with the detailed dynamics by following the time development of the condensate density and the phase simultaneously, and presents a number of previously unpublished results. Although the dissipation is treated phenomenologically in the GP equation, the simulation reproduces the experimental results very well.

The results show that the generation of surface ripples is also achieved by the instability of negative eigenvalue modes, i.e., Landau instability, and the following time development certainly leads to vortex penetration into the condensate. The experimental results on vortex nucleation by the ENS group [1,5] can be understood by taking into account both the dynamical instability and the Landau instability. This is described in Sec. IV E.

A. Phenomenological dissipative equation

Before discussing the detailed dynamics, we make some comments on the dissipation. As in the previous study [14], the dissipation is treated phenomenologically in the GP equation. The time derivative term of Eq. (7) is modified as

$$(i-\gamma)\frac{\partial\psi}{\partial t}=\left[-\left(\frac{\partial^2}{\partial x^2}+\frac{\partial^2}{\partial y^2}\right)+\frac{1}{4}\{(1+\epsilon_x)x^2+(1+\epsilon_y)y^2\}\right.$$
$$\left.-\mu+C|\psi|^2-\Omega L_z\right]\psi, \qquad (28)$$

where the dimensionless parameter γ describes the degree of dissipation. This form of the dissipative equation follows the study of Choi *et al.* [36] and that of other superfluid systems [37]. Choi *et al.* determined the value of γ to be 0.03 by fitting their theoretical results with the MIT experiments on collective damped oscillations [38]. Thus, we also use $\gamma=0.03$ throughout this work. Since this dissipative term is much smaller than other terms in the GP equation, a small variation of γ does not change the dynamics qualitatively but only modifies the relaxation time scale.

The phenomenological dissipative Eq. (28) may be related to the recent numerical work by Jackson and Zaremba [39] on the coupled dynamics of a condensate and a noncondensate. Their simulation is based on the the generalized GP equation at finite temperatures

$$i\hbar\frac{\partial\Psi}{\partial t}=\left(-\frac{\hbar^2\nabla^2}{2m}+V_{\rm trap}+gn+2g\tilde{n}-i\Gamma\right)\Psi. \qquad (29)$$

This equation was derived by Zaremba, Nikuni, and Griffin [40], where $n(\mathbf{r},t)=|\Psi(\mathbf{r},t)|^2$ is the condensate density and $\tilde{n}(\mathbf{r},t)$ is the noncondensate density. The dynamics of the noncondensate was described by the Boltzmann kinetic equation for the distribution function of the noncondensate atoms. The noncondensate atoms are assumed to possess the single-particle Hartree-Fock spectrum in their formulation. The numerical simulation by Jackson and Zaremba [39] well explains the experimental results by Maragò *et al.* [41] and Jin *et al.* [42].

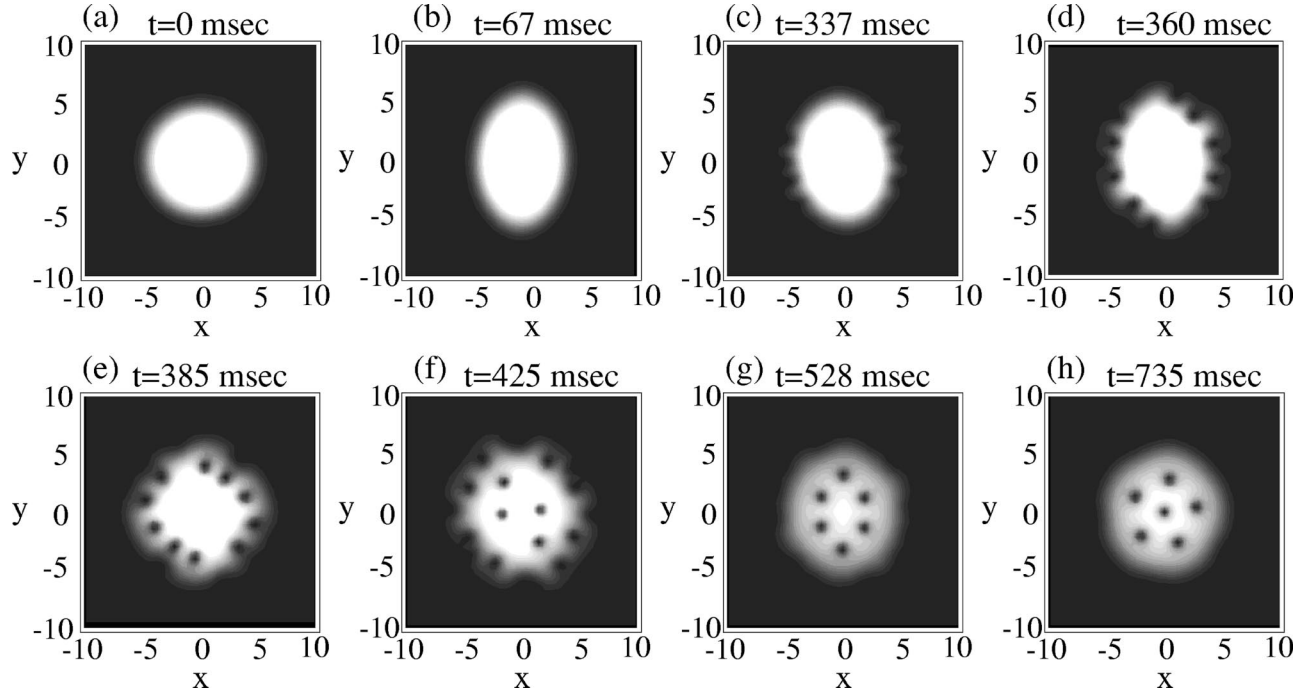

FIG. 5. Time development of the condensate density $|\psi|^2$ after the trapping potential suddenly begins to rotate at $t=0$ with $\Omega=0.7\omega_\perp$.

Equation (28) can be derived from Eq. (29) with some additional approximations. We treat the noncondensate as being in static thermal equilibrium, and neglect the mean field of the noncondensate under the assumption $n \gg \tilde{n}$. Then, the dissipation of the condensate motion is associated with the term $\Gamma(\mathbf{r},t)=(\hbar/2n)\Gamma_{12}=(\hbar/2n)\int\{d\mathbf{p}/(2\pi\hbar)^3\}C_{12}$ with the collision integral C_{12} between the condensate and noncondensate atoms. Under the local equilibrium distribution of the thermal atoms, Γ_{12} is proportional to the difference of the local chemical potential between condensate and noncondenate as $\Gamma_{12} \propto \mu_{\rm nc}(\mathbf{r},t)-\mu(\mathbf{r},t)$ [40]. Approximating $\mu(\mathbf{r},t)\Psi \simeq -i\hbar(\partial\Psi/\partial t)$ [44], we obtain

$$(i-\gamma)\hbar\frac{\partial\Psi}{\partial t}=\left(-\frac{\hbar^2}{2m}\nabla^2+V_{\rm trap}+g|\Psi|^2-i\gamma\mu_{\rm nc}\right)\Psi. \tag{30}$$

Compared with Eq. (28), the chemical potential of this equation is replaced by that of noncondensate $\mu_{\rm nc}$, yielding the imaginary term $i\gamma\mu_{\rm nc}$. Note that the relation $\mu=\mu_{\rm nc}$ is satisfied for the equilibrium condensate. If the space and time dependence of $\mu_{\rm nc}$ is neglected, this equation becomes Eq. (28) by the transformation $\Psi \to \Psi e^{-i\mu_{\rm nc}t/\hbar}$ and $\mu_{\rm nc}\to\mu$.

The time development of Eq. (28) conserves neither the norm of the wave function nor the energy. In our simulation, the chemical potential μ is adjusted at each time step in order to conserve the norm and to decrease the total energy monotonically. Recently, Eq. (30) was also derived by Gardiner *et al.* by another approach [45], applied to the simulation of vortex lattice formation from a rotating thermal cloud [46]. They made the numerical simulation with the fixed chemical potential, finding that the norm of Ψ decreased or increased as the system evolved. In actual experiments, such a loss in the number of condensate atoms is caused by the rotation-induced heating [3], so that the generated thermal component might affect the dissipative dynamics of the vortex generation. However, under the phenomenological model, the change of the norm is only a few percent, be the chemical potential fixed or not. The detailed quantitative study of a loss of atoms is beyond the scope of this paper; our treatment using the fixed chemical potential is adequate to describe the actual dissipative dynamics.

The assumption of the static noncondensate may be applicable to the experimental condition in Refs. [1–3,5]. According to the estimation by Guery-Odelin [47], the spin up time for the whole noncondensed atoms to catch up with the rotating trap is about 15 sec in collisionless regime. Since the typical time for the vortex formation of the condensate is a few hundred milliseconds, the condensate motion is separated from the noncondensate one under the rotating perturbation. However, the dynamic coupling via the mean-field interaction between condensate and noncondenate causes the condensate motion to be damped (known as Landau damping), which is not included in Eq. (28).

The value of γ is estimated by following the formulation for a uniform Bose gas [43]. The parameter γ, in which length and energy are scaled by a_h and $\hbar\omega_\perp$, has the form

$$\gamma=16\sqrt{2\pi}An a^3\left(\frac{a_h}{a}\right)\sqrt{\frac{T_C}{T}}\sqrt{\frac{\hbar\omega_\perp}{k_BT}}. \tag{31}$$

Here A is a factor of order unity for $T>0.5T_C$ and approaches zero as $T\to 0$. Using typical experimental parameters, for example, $T=0.5T_C$, $T_C=500$ nK, $a=5.5$ nm, n

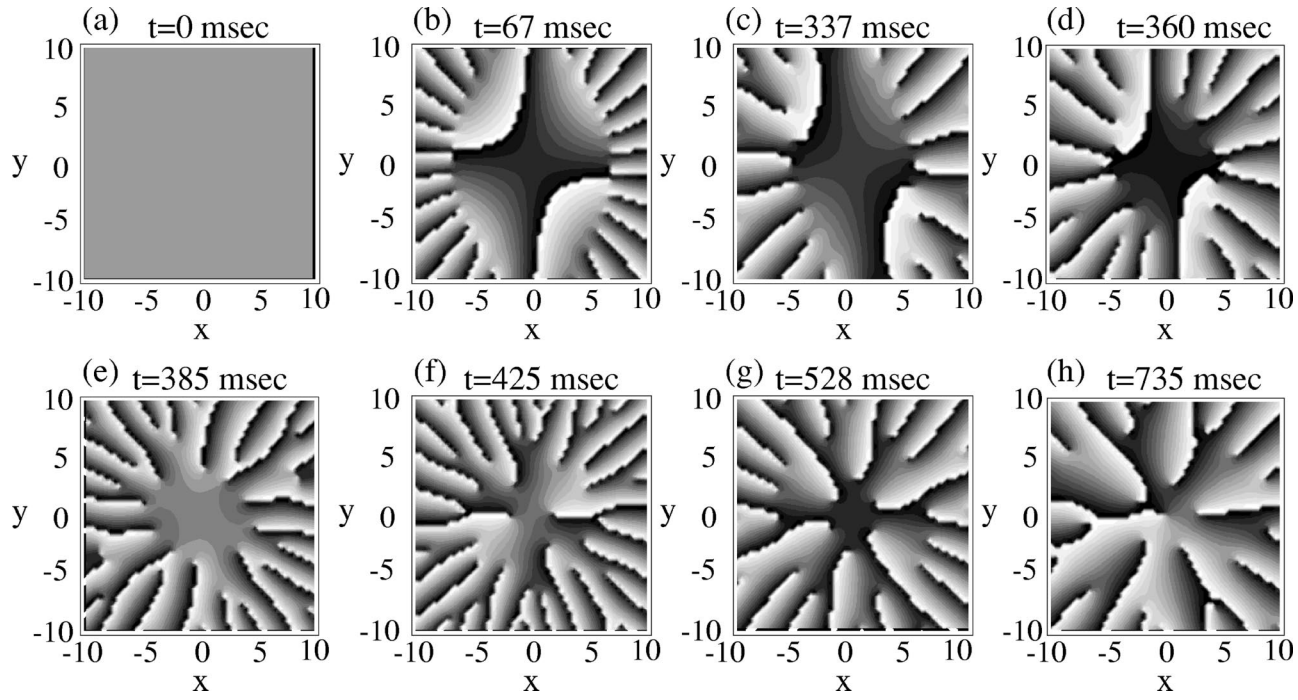

FIG. 6. Phase profiles of ψ corresponding to the density profiles of Fig. 5. The value of the phase changes continuously from 0 (black) to 2π (white). The discontinuous lines between black and white correspond to the branch cut of the complex plane, and their edges represent quantized vortices. The unit of length is the same as that of Fig. 5.

$\sim 10^{14}$ cm^{-3}, and $\omega_\perp = 100 \times 2\pi$ Hz, we obtain $\gamma \sim A \times 10^{-2}$ which is consistent with 0.03 used in this paper.

B. Dynamics from a nonvortex state to a vortex state

Using Eq. (28), we discuss the dynamics of vortex lattice formation in more detail. As in the preceeding section, a sudden switch on of rotation is made for the condensate with $C = 500$. Figure 5 shows the time development of the condensate density $|\psi(x,y,t)|^2$ for $\Omega/\omega_\perp = 0.7$ [48]. Initially, the condensate undergoes a quadrupole oscillation, but the oscillation is damped due to dissipation. After a few hundred milliseconds, the boundary surface of the condensate becomes unstable, generating the surface ripples that propagate along the surface as shown in Fig. 5(c). The excitations are likely to occur on the surface whose curvature is low, i.e., parallel to the longer axis of the ellipse. Then the waves on the surface develop into the vortex cores in a very short time [Figs. 5(d) and 5(e)]. As is well known in the study of rotating superfluid helium [34,35], the rotating drive pulls vortices toward the rotation axis, while repulsive interaction between vortices tends to push them apart; this competition yields a vortex lattice whose vortex density depends on the rotation frequency. In the presence of dissipation, six vortices enter the condensate, eventually forming a vortex lattice. As the vortex lattice is being formed, the axisymmetry of the condensate shape is recovered.

The rotating potential $V_{\rm rot}$ has even parity with respect to the coordinate. Accordingly, the number of the generated vortices is always even. To remove this restriction, we introduced an infinitesimal artificial perturbation with odd parity in $V_{\rm trap}$. This perturbation allows the system to develop into an a fivefold symmetric steady state as shown in Fig. 5(h), the energy of which is lower than that in Fig. 5(g). It takes a few hundred milliseconds for the transition from Fig. 5(g) to 5(h).

The corresponding time development of the phase of $\psi(x,y,t)$ is shown in Fig. 6. As seen in the energy-conserving dynamics, as soon as the rotation starts, the phase field inside the condensate takes the form of quadrupolar flow $\theta(x,y) = \alpha xy + \text{const}$, and just outside the Thomas-Fermi boundary there appear ghost vortices; for example, Fig. 6(b) shows about 20 vortices. Ghost vortices move toward the rotation axis, but their invasion into the condensate is prevented at the Thomas-Fermi boundary. However, as the surface ripples are generated, the ghost vortices start to penetrate the condensate. There takes place the selection of the defects to penetrate, because their further invasion costs energy and angular momentum. For example, Fig. 6 shows that six vortices enter the condensate and form a lattice, while other excessive vortices are repelled and escape to the outside.

As seen from Fig. 5, vortex invasion is likely to occur on the surface parallel to the longer axis of the ellipse. This is simply understood by the velocity field of the elliptic condensate $\mathbf{v} = \nabla \alpha xy = (\alpha y, \alpha x)$ as seen in Fig. 6(b). Near the condensate surface parallel to the longer axis of an ellipse, this velocity field has the same direction as the velocity field produced by the ghost vortices. There the additive velocity field $\mathbf{v}$ works as an attractive force that pulls the ghost vortices into the condensate. On the other hand, the velocities of

the condensate and the ghost vortices have the opposite direction near the surface parallel to the shorter axis, where the condensate dislikes the invasion of the ghost vortices. Therefore, the vortices enter the condensate from the surface parallel to the longer axis.

Figure 7 shows the time evolution of the deformation parameter and that of the angular momentum per atom $\ell_z/\hbar = \int dxdy\psi^*(L_z/\hbar)\psi$ in our dynamics of Figs. 5 and 6. They very well reproduce the experimental results of Ref. [5]. Before 300 msec, both α and $\ell_z/\hbar$ undergo damped oscillations. When vortices enter the condensate, α falls abruptly to a value below 0.05 and $\ell_z/\hbar$ increases to 4 reflecting the number of the generated vortices.

The final equilibrium value of ℓ_z depends on the number of the vortices that form a lattice. Figure 8 shows the dependence of the number of vortices on the frequency $\Omega/\omega_\perp$ and the angular momentum per atom $\ell_z/\hbar$ for $C=250$, 500, and 1500 at 800 ms after the rotation starts. The increase in C stabilizes the lattices of more vortices for the same frequency, and reduces the critical frequency at which the first vortex appears. Note that the value of $\ell_z/\hbar$ is about a half of the number of vortices. This is understood by the simple model in which the condensate with a vortex lattice makes a rigid-body rotation. Then the mean angular momentum per atom at $r=\sqrt{x^2+y^2}$ is $\ell_z/\hbar = m\Omega r^2$. The average of the angular momentum per atom averaged over the whole condensate is given by

$$\langle \ell_z/\hbar \rangle = \frac{\int |\psi|^2(\ell_z/\hbar)d\mathbf{r}}{\int |\psi|^2 d\mathbf{r}}. \tag{32}$$

Assuming the spatially homogeneous density, we obtain $\langle \ell_z/\hbar \rangle = m\Omega R^2/2\hbar$ with the typical radius R of the condensate. In the limit of a rigid-body rotation, the number of vortices N_v^{lattice} at the rotation frequency Ω is given by Feynman's rule,

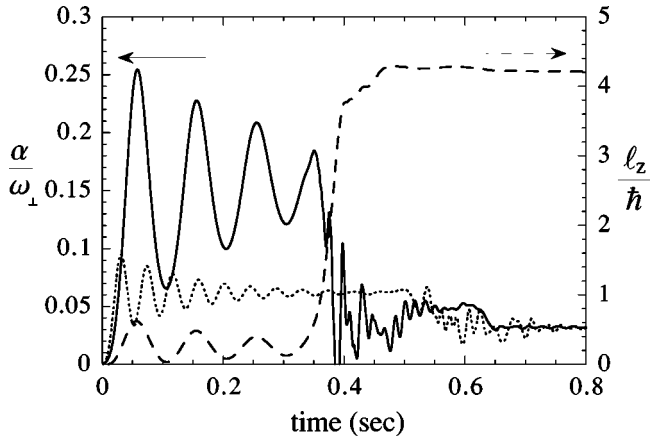

FIG. 7. Time evolution of the distortion parameter α (solid curve) and the angular momentum per atom $\ell_z/\hbar$ (dashed curve) in the dynamics of Figs. 5 and 6. The dotted curve shows α for the dynamics starting from the initial state with one vortex.

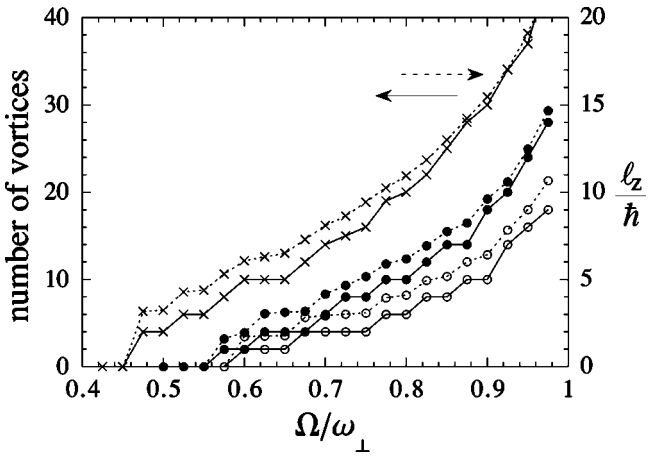

FIG. 8. The number of vortices (solid curve) and angular momentum per atom (dotted curve) versus $\Omega/\omega_\perp$, for $C=250$ (with empty circles), 500 (with filled circles), and 1500 (with crosses).

$$N_v^{\text{lattice}} = \pi R^2 n_v = \pi R^2 \frac{2\Omega}{\kappa} = \frac{m\Omega R^2}{\hbar}, \tag{33}$$

where n_v represents the number of vortices per unit area and κ the quanta of circulation. Hence, one obtains $\langle \ell_z/\hbar \rangle = N_v^{\text{lattice}}/2$. The numerical result better agrees with this estimation for larger Ω and larger C because the condensate with a dense vortex lattice mimics a rigid-body rotation [49]. The small disagreement may be attributed to a small deviation from Feynman's rule and the inhomogeneous density.

C. Dynamics starting from an initial state with one vortex: Metastable state

Next, we discuss the time evolution starting from a one-vortex state. As seen from Figs. 5 and 6, as soon as the rotation is turned on to the irrotational condensate, the condensate makes the quadrupole deformation and its phase takes the form $\theta(x,y)=\alpha xy+\text{const}$. This behavior will be changed if the dynamics starts from the initial state with one vortex that has already the circulating phase field. References [19] and [20] discuss the stability of the condensate with a vortex against the quadrupole mode. To investigate this problem, we prepare an initial state with one vortex for $C=500$ and $\Omega=0.4\omega_\perp$ that is larger than the thermodynamical critical frequency for the stabilization of a one-vortex state [8,9,11,24]. We then start to rotate the system with $\Omega=0.7\omega_\perp$ as before. The time evolution of the phase is shown in Fig. 9. The numerical simulation reveals the nontrivial structure of the phase field; at the center of the condensate the phase maintains the circulation carried by an original vortex, while in the outer region the phase makes the quadrupolar flow [Fig. 9(b)]. Therefore, the condensate with one vortex also makes quadrupole deformation. The corresponding time evolution of the deformation parameter α is shown in Fig. 7 by the dotted curve. The small amplitude of α compared to the previous result is due to the shift of the resonance frequency of the quadrupole mode because of the presence of a vortex [50].

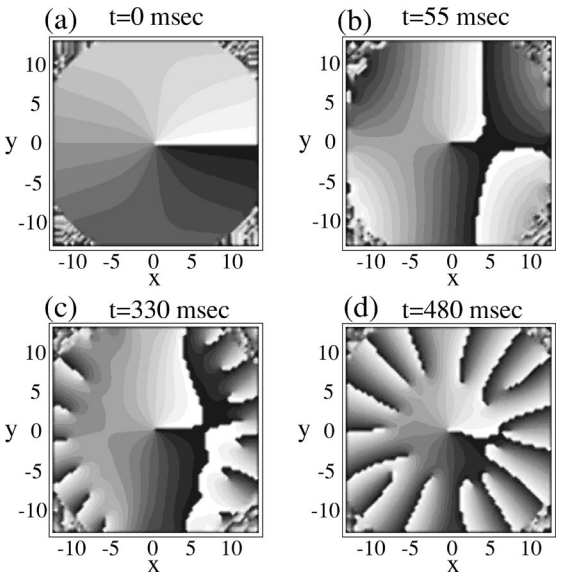

FIG. 9. Phase profile of the simulation starting from one-vortex state.

After that, the dynamics follows the same process as before. The final steady state is the lattice with seven vortices. This state is energetically higher than that of Fig. 5(h) with six vortices. Therefore, by starting from different initial states, one can obtain various metastable states with different configuration of a vortex lattice, as studied in rotating superfluid helium [34].

D. Surface ripple excitation via the Landau instability

As stated above, vortices are initially generated outside the Thomas-Fermi boundary of the condensate, where the energy cost to create phase singularities is small because of the extremely low density. However, their penetration into the condensate was accomplished with the help of the surface ripples, induced by the instabilities in the nonvortex state. The quasiparticle projection method is useful to reveal the instability of the surface mode in this dissipative dynamics. Note that the time derivative term of Eqs. (22) and (23) is modified as $(i-\gamma)\partial/\partial t$. Then, the nonvortex state becomes unstable when at least one excitation frequency $\tilde{\omega}_l = \omega_l - l\Omega + O(\epsilon)$ becomes negative, causing the exponential growth like $b_l(t) \sim e^{-\gamma\tilde{\omega}_l t}$. Isoshima and Machida examined that the instability associated with the negative excitation frequency gives rise to the vortex formation [8], and calculated the critical frequency Ω_c at which the first vortex appears within the Bogoliubov theory. García-Ripoll and Pérez-García calculated Ω_c under more realistic conditions [11]. The critical frequency can be expressed by the Landau criterion applied to the rotating BECs [7]:

$$\Omega_c = \min\left(\frac{\omega_l}{l}\right). \tag{34}$$

The angular momentum l_c that yields Ω_c takes a value larger than 4 with the parameter used in experiments [7,8,15]; for $C=500$ used in this paper, $l_c=8$ and $\Omega_c=0.5\omega_\perp$.

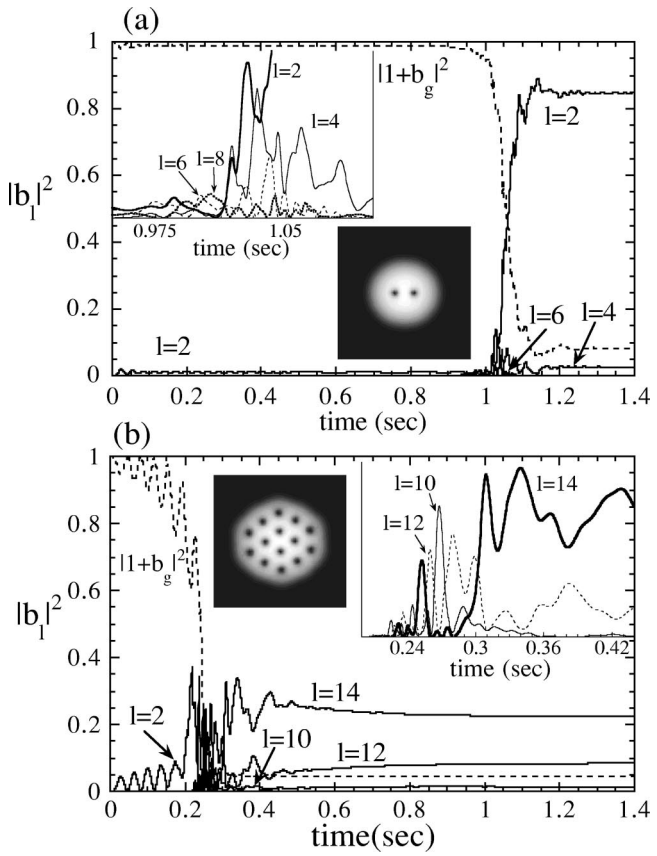

FIG. 10. Time evolution of the surface-mode amplitude $|b_l|^2$ in the dissipative dynamics for (a) $\Omega=0.57\omega_\perp$ and (b) $\Omega=0.86\omega_\perp$ under the same condition in Sec. IV. In (b), we plot only modes with $l=2,10,12$, and 14, which are important in the discussion. The inset shows the density profile of the final steady state. The other inset in (b) shows $|b_{10}|^2$, $|b_{12}|^2$, and $|b_{14}|^2$ near $t=0.3$ sec.

Our simulation confirms that this instability actually leads to the generation of vortices, where the hollows of the surface ripples always evolve into the vortex cores. The vortex core near the condensate surface has the size of the coherence length ξ determined by the local density. The number of the vortices generated at the condensate surface may be approximately given by $N_v^{\rm surf} \sim 2\pi R/\xi$. The numerical solution shows $2\pi R/\xi$ is nearly equal to l_c. This is understood by the fact that the surface mode with l_c has the wavelength of the order of ξ as discussed in Ref. [7].

Note that $N_v^{\rm surf}$ differs generally from the number of vortices $N_v^{\rm lattice}$, depending on Ω, in an eventual vortex lattice. This fact classifies the dynamics of a vortex invasion into two regimes. When $N_v^{\rm surf} > N_v^{\rm lattice}$, the vortices that invade the condensate are chosen from $N_v^{\rm surf}$ vortices generated at the surface and form a lattice following the dissipative vortex dynamics, the extra $N_v^{\rm surf} - N_v^{\rm lattice}$ vortices being expelled out [35]. This dynamics is shown in Fig. 10(a) in terms of the quasiparticle populations for $N_c \simeq l_c = 8$ and $N_v^{\rm lattice}=2$; for $\Omega=0.57\omega_\perp$, the excitation frequencies ω_l with $l=4$–14 are negative. At the moment the vortices are about to enter the condensate ($t\sim 1.0$ sec), the modes with $l=4$, 6, and 8 (with $|b_l|^2 > 0.02$) are excited. These modes rapidly decay as two

vortices penetrate into the condensate. After the vortex invasion, the final growth of the projected population of the $l=2$ mode reflects the phase structure in the surface region of the lattice with two vortices.

On the other hand, if $N_{\rm v}^{\rm surf}<N_{\rm v}^{\rm lattice}$, the number of the vortices first generated at the condensate surface is not sufficient to form a final lattice, so that successive invasion of vortices is needed. This situation is shown in Fig. 10(b) with $N_{\rm v}^{\rm lattice}=14$. The frequency $\tilde{\omega}_2$ is already negative at $\Omega=0.86\omega_\perp$, which causes the exponential growth of $|b_2|^2$. When the condensate deforms elliptically at $t\sim 0.2$ sec, many kinds of surface modes are excited violently. Then the quasiparticle populations with high angular momentum [$l=10$, 12, and 14 are plotted in Fig. 10(b)] oscillate during a short time after this burst. Finally, $|b_{14}|^2$ grows when 14 vortices enter the condensate completely. Note that the $l=14$ mode does not grow shortly after the burst, but it grows gradually through the excitation of the lower angular momentum modes.

E. Relation between dynamical instability and Landau instability in the experiments on vortex nucleation

For an irrotational BEC subject to rotation, we have clarified by the numerical simulation of the GP equation that there exist two instabilities that are relevant for vortex generation. The dynamical instability appears when the quadrupole surface mode is resonantly excited. The Landau instability associated with the negative excitation frequency is effective only in the presence of the dissipation. In this section, we discuss which instability is more important for actual vortex lattice formation by referring to the experimental results.

In the experiments [1,2,5], the authors observed that vortices are nucleated most frequently near $\Omega=0.7\omega_\perp$. Thus, vortices are generated when the condensate becomes resonant with the rotating perturbation that excites a quadrupole mode. These results appear to support the dynamical instability scenario by Sinha and Castin [12]. However, they also observed the vortices at lower off-resonant frequencies, which cannot be understood by the dynamical instability. On the other hand, the critical frequency at which the first vortices appear is extensively discussed by several authors, based on the Landau criterion [7,8,11,15–18]. The relation between the dynamical instability and Landau instability is still controversial; thus we discuss these relations in the range of on- and off-resonant frequency separately.

In the resonant regime $0.72<\Omega<0.78$, the surface ripples are excited, but the dissipation is necessary for vortices to penetrate into the condensate. Here the dissipation may originate in the thermal component, which should be almost negligible in the experiment of the atomic gas at very low temperatures. However, in the dynamical process of a condensate, there is a possibility that the thermal component will be produced under a strong perturbation. The experimental result of ENS [1] may be explained as follows. Consider a situation in which there is almost no dissipation at very low temperatures, namely, Landau instability does not work there. In a quadrupole resonance, however, the dynamical instability causes stochasticity in condensate oscillations, leading to the creation of the thermal component [30–32]. Indeed, Hodby *et al.* in Oxford has reported that temperature of the system increases from $0.5T_c$ to $0.8T_c$ during the vortex formation procedure [3]. The time spent in this process is determined by the growth time of the dynamical instability, which is expected to be about 100 msec [12]. Then, the created thermal component makes the dissipation effective, so the vortices can penetrate into the condensate via the Landau instability. To make clear this hypothesis, we need the analysis beyond the GP equation and leave this issue for future study.

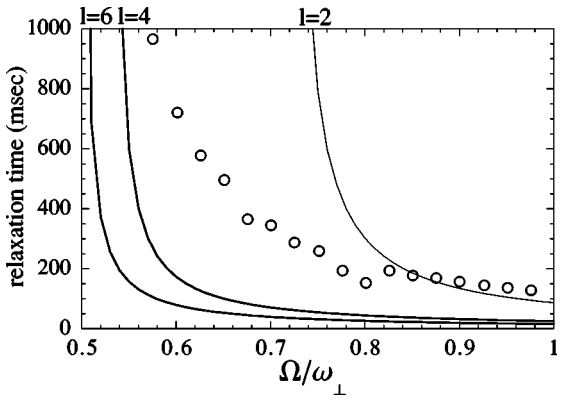

FIG. 11. The circles represent the relaxation time of vortex lattice formation by the numerical simulation for $C=500$ and $\gamma=0.03$. Thin solid curves show the $\tau_l=-\{\gamma(\omega_l-l\Omega)\omega_\perp\}^{-1}$ for $l=2$, 4, and 6 obtained from Eq. (16)

In the off-resonant regime, a condensate makes only a stable quadrupole oscillation without dissipation. However, our results show that vortices may be generated at frequencies beyond Ω_c whenever finite dissipation works. Therefore, if we make the experiment in which the temperature is high enough that the dissipation works effectively, it is possible to observe the critical frequency given by Landau criterion. For the weakly anisotropic rotating potential used in the ENS experiments and in this paper, excitations of high-l modes can be made only through the $l=2$ excitation, so that it takes very long time for the vortex formation near the critical frequency. Figure 11 represents the relaxation time for vortex lattice formation in our simulation with $C=500$ and $\gamma=0.03$ ($\Omega_c=0.5$). Here the relaxation time is determined as the time needed for the angular momentum of the system to become half of the final equilibrium value. We also show the growth time via Laudau instability $\tau_l=-\{\gamma(\omega_l-l\Omega)\omega_\perp\}^{-1}$ for $l=2$, 4, and 6. For $\Omega<0.7\omega_\perp$, where $\omega_2-2\Omega>0$, the relaxation time is longer than τ_l with $l=4, 6, 8, \ldots$, because high-l modes are only excited through the $l=2$ mode which has no instability. Near the critical frequency Ω_c, one finds a very long relaxation time about 1 sec. As Ω increases higher than $0.8\omega_\perp$, where $\omega_2-2\Omega<0$, the relaxation time matches τ_2. The ENS group found no vortices in the off-resonant range near Ω_c, presumably because the observation time was not long enough (>1 sec is need for vortex nucleation in this regime).

V. CONCLUSIONS

We investigate the detailed dynamics of a rotating BEC in a trapped condensate following the sudden turn on of rotation. The numerical analysis of the two-dimensional GP equation shows a series of nonlinear dynamics that had not been clarified so much. In the energy-conserving dynamics, we study the quadrupole oscillation induced by an anisotropic rotating potential, and the time development of excitation modes by the quasiparticle projection method. In the resonance range of the quadrupole mode, the large amplitude oscillation causes via the dynamical instability the nonlinear mode coupling that leads to the excitations of higher-energy mode. This nonlinear process leads to generation of surface ripples, but not to nucleation of vortices. In the dissipative dynamics, the vortex lattice formation is studied in detail. The vortex penetration into the condensate is achieved by the surface modes excitation with negative frequencies in the rotating frame, so that the critical frequency for vortex generation is determined by the Landau instability. Two possible instabilities for vortex generation are discussed by comparison with the experiments. While the dynamical instability helps induce vortex nucleation and may increase a thermal component, such an instability alone cannot explain the experimental results. Vortex nucleation and penetration are eventually caused by the Landau instability.

In this paper, we confine ourselves to the rotating laser beam whose size is larger than the condensate size. This fact allows us to use the form of the potential in Eq. (3) which excites the collective surface mode. Recently, Raman *et al.* studied vortex formation by using a narrow stirring beam with two-point patterns, and found no resonance in the number of nucleated vortices [2]. In addition, they observe vortices at lower rotation frequencies than Ω_c of Eq. (34). In this case, the mechanism of vortex nucleation is presumably due to the local instability of the superflow around a narrow potential rather than to the instabilities of collective surface modes. Numerical simulations of the GP equation show that the vortex pairs are created by the object that moves faster than a certain critical speed [51]. Such an excitation is expected to lead to the heating of the condensate [52], thereby a vortex lattice being formed. This different mechanism may make it possible to stabilize a vortex lattice below the critical frequency Ω_c given by the Landau criterion of the surface mode.

A similar competition between the dynamical instability and the Landau instability has been found in the center-of-mass oscillation of a BEC in a one-dimensional optical lattice [53]. They observed the critical superfluid speed above which the dissipative dynamics starts. Its main features, including the parameter range of instability, can be explained by the simulation of the dissipationless GP equation [54], which means that the observed phenomena may be caused by a dynamical instability. However, the ensuring development of a condensate is not explained by the dynamical instability alone; the dissipation-assisted instability such as the Landau instability is necessary to describe the dynamics [53]. These problems on the dissipative dynamics of BECs associated with vortex lattice formation offer a unique testing ground for a much-needed framework beyond the GP equation.

ACKNOWLEDGMENTS

We would like to thank T. Nikuni for useful discussions. We also thank T. Iida for instructive comments on this work. M.T. acknowledges support from a Grant-in-Aid for Scientific Research (Grant No. 12640357) by the Japan Society for the Promotion of Science. M.U. acknowledges support from a Grant-in-Aid for Scientific Research (Grant No. 11216204) by the Ministry of Education, Culture, Sports, Science and Technology of Japan, and by the Toray Science Foundation.

[1] K.W. Madison, F. Chevy, W. Wohlleben, and J. Dalibard, Phys. Rev. Lett. **84**, 806 (2000); F. Chevy, K.W. Madison, and J. Dalibard, *ibid.*, **85**, 2223 (2000).
[2] J.R. Abo-Shaeer, C. Raman, J.M. Vogels, and W. Ketterle, Science **292**, 476 (2001); C. Raman, J.R. Abo-Shaeer, J.M. Vogels, K. Xu, and W. Ketterle, Phys. Rev. Lett. **87**, 210402 (2001).
[3] E. Hodby, G. Hechenblaikner, S.A. Hopkins, O.M. Maragó, and C.J. Foot, Phys. Rev. Lett. **88**, 010405 (2002).
[4] P.C. Haljan, I. Coddington, P. Engels, and E.A. Cornell, Phys. Rev. Lett. **87**, 210403 (2001).
[5] K.W. Madison, F. Chevy, V. Bretin, and J. Dalibard, Phys. Rev. Lett. **86**, 4443 (2001).
[6] For a review, see, for example, A.L. Fetter and A.A. Svidzinsky, J. Phys.: Condens. Matter **13**, R135 (2001).
[7] F. Dalfovo, S. Giorgini, M. Guilleumas, L. Pitaevskii, and S. Stringari, Phys. Rev. A **56**, 3840 (1997); F. Dalfovo and S. Stringari, *ibid.* **63**, 011601 (2001).
[8] T. Isoshima and K. Machida, Phys. Rev. A **60**, 3313 (1999).
[9] D.L. Feder, C.W. Clark, and B.I. Schneider, Phys. Rev. A **61**, 011601 (1999).
[10] D.L. Feder, A.A. Svidzinsky, A.L. Fetter, and C.W. Clark, Phys. Rev. Lett. **86**, 564 (2001).
[11] J.J. García-Ripoll and V.M. Pérez-García, Phys. Rev. A **63**, 041603(R) (2001).
[12] S. Sinha and Y. Castin, Phys. Rev. Lett. **87**, 190402 (2001).
[13] A. Aftalion and Q. Du, Phys. Rev. A **64**, 063603 (2001).
[14] M. Tsubota, K. Kasamatsu, and M. Ueda, Phys. Rev. A **65**, 023603 (2002).
[15] J.R. Anglin, Phys. Rev. Lett. **87**, 240401 (2001).
[16] A.E. Muryshev and P.O. Fedichev, e-print cond-mat/0106462.
[17] T. Mizushima, T. Isoshima, and K. Machida, Phys. Rev. A **64**, 043610 (2001).
[18] T.P. Simula, S.M.M. Virtanen, and M.M. Salomaa, Phys. Rev. A **66**, 035601 (2002).
[19] J.E. Williams, E. Zaremba, B. Jackson, T. Nikuni, and A. Griffin, Phys. Rev. Lett. **88**, 070401 (2002).
[20] M. Kraemer, L. Pitaevskii, S. Stringari, and F. Zambelli, Laser Phys. **12**, 113 (2002).
[21] J.R. Anglin, Phys. Rev. A **65**, 063611 (2002).
[22] S.A. Morgan, S. Choi, K. Burnett, and M. Edwards, Phys. Rev. A **57**, 3818 (1998).

[23] E. Fermi, J. Pasta, and S. Ulam, in *Collected Papers of Enrico Fermi*, edited by E. Segré (University of Chicago Press, Chicago, 1965).
[24] J.J. García-Ripoll and V.M. Pérez-García, Phys. Rev. A **64**, 053611 (2001).
[25] A. Aftalion and T. Riviere, Phys. Rev. A **64**, 043611 (2001).
[26] P. Rosenbusch, V. Bretin, and J. Dalibard, Phys. Rev. Lett. **89**, 200403 (2002).
[27] W. H. Press *et al.*, *Numerical Recipes in C* (Cambridge University Press, Cambridge, 1988).
[28] A. Recati, F. Zambelli, and S. Stringari, Phys. Rev. Lett. **86**, 377 (2001).
[29] S. Stringari, Phys. Rev. Lett. **77**, 2360 (1996).
[30] Y. Kagan, E.L. Surkov, and G.V. Shlyapnikov, Phys. Rev. A **55**, R18 (1997).
[31] A. Sinatra, P.O. Fedichev, Y. Castin, J. Dalibard, and G.V. Shlyapnikov, Phys. Rev. Lett. **82**, 251 (1999).
[32] P. Villain and M. Lewenstein, Phys. Rev. A **62**, 043601 (2000).
[33] A. Smerzi, S. Fantoni, S. Giovanazzi, and S.R. Shenoy, Phys. Rev. Lett. **79**, 4950 (1997); S. Raghavan, A. Smerzi, S. Fantoni, and S.R. Shenoy, Phys. Rev. A **59**, 620 (1999).
[34] L.J. Campbell and R.M. Ziff, Phys. Rev. B **20**, 1886 (1979).
[35] M. Tsubota and H. Yoneda, J. Low Temp. Phys. **101**, 815 (1995).
[36] S. Choi, S.A. Morgan, and K. Burnett, Phys. Rev. A **57**, 4057 (1998). In this paper, the physical interpretation of the damping mechanism is the relaxation process of the thermal particles into the condensate. Thus, γ represents the rate at which the excited components turn into the condensate.
[37] For example, I. Aranson and V. Steinberg, Phys. Rev. B **54**, 13 072 (1996).
[38] M.-O. Mewes, M.R. Andrews, N.J. van Druten, D.M. Kurn, D.S. Durfee, C.G. Townsend, and W. Ketterle, Phys. Rev. Lett. **77**, 988 (1996).
[39] B. Jackson and E. Zaremba, Phys. Rev. Lett. **87**, 100404 (2001); **88**, 180402 (2002).
[40] E. Zaremba, T. Nikuni, and A. Griffin, J. Low Temp. Phys. **116**, 277 (1999).
[41] O. Maragò, G. Hechenblaikner, E. Hodby, and C. Foot, Phys. Rev. Lett. **86**, 3938 (2001).
[42] D.S. Jin, M.R. Matthows, J.R. Ensher, C.E. Wieman, and E.A. Cornell, Phys. Rev. Lett. **78**, 764 (1997).
[43] Substituting $\Psi(\mathbf{r},t)=\sqrt{n(\mathbf{r},t)}e^{i\theta(\mathbf{r},t)}$ into the GP equation, we obtain

$$\frac{\partial n}{\partial t}=-\nabla(n\mathbf{v}_c),$$

$$\hbar\frac{\partial\theta}{\partial t}=\mu+\frac{1}{2}mv_c^2,$$

where $\mu(\mathbf{r},t)=(\hbar^2\nabla^2\sqrt{n})/(2m\sqrt{n})+V_{\rm trap}+gn$ and $\mathbf{v}_c=\hbar\nabla\theta/m$. Using these relations,

$$-i\hbar\frac{\partial\Psi}{\partial t}=-i\hbar\frac{\partial\sqrt{n}}{\partial t}e^{i\theta}+\hbar\Psi\frac{\partial\theta}{\partial t}$$

$$=\left(i\hbar\frac{\nabla(n\mathbf{v_c})}{2}n+\frac{mv_c^2}{2}+\mu\right)\Psi.$$

If we assume $|\mathbf{v_c}|$ and the gradient of the density to be small, the approximation $\mu(\mathbf{r},t)\Psi\simeq-i\hbar(\partial\Psi/\partial t)$ is attainable.
[44] C.W. Gardiner, J.R. Anglin, and T.I.A. Fudge, J. Phys. B **35**, 1555 (2002).
[45] A.A. Penckwitt, R.J. Ballagh, and C.W. Gardiner, Phys. Rev. Lett. **89**, 260402 (2002).
[46] D. Guery-Odelin, Phys. Rev. A **62**, 033607 (2000).
[47] T. Nikuni, E. Zaremba, and A. Griffin, Phys. Rev. Lett. **83**, 10 (1999).
[48] You can see the animation of this dynamics in http://matter.sci.osaka-cu.ac.jp/bsr/vortexex-e.html
[49] D.L. Feder and C.W. Clark, Phys. Rev. Lett. **87**, 190401 (2001).
[50] F. Zambelli and S. Stringari, Phys. Rev. Lett. **81**, 1754 (1998).
[51] T. Frisch, Y. Pomeau, and S. Rica, Phys. Rev. Lett. **69**, 1644 (1992); B. Jackson, J.F. McCann, and C.S. Adams, *ibid.* **80**, 3903 (1998).
[52] C. Raman, M. Köhl, R. Onofrio, D.S. Durfee, C.E. Kuklewicz, Z. Hadzibabic, and W. Ketterle, Phys. Rev. Lett. **83**, 2502 (1999).
[53] S. Burger, F.S. Cataliotti, C. Fort, F. Minardi, M. Inguscio, M.L. Chiofalo, and M.P. Tosi, Phys. Rev. Lett. **86**, 4447 (2001); **89**, 088902 (2002).
[54] B. Wu and Q. Niu, Phys. Rev. Lett. **89**, 088901 (2002).